HHS Public Access

Author manuscript

*Curr Biol*. Author manuscript; available in PMC 2023 July 05.

Published in final edited form as:

*Curr Biol*. 2020 July 20; 30(14): 2707–2715.e3. doi:10.1016/j.cub.2020.05.018.

# Category Selectivity for Face and Scene Recognition in Human Medial Parietal Cortex

**Oscar Woolnough**[1,2], **Patrick S. Rollo**[1,2], **Kiefer J. Forseth**[1,2], **Cihan M. Kadipasaoglu**[1,3], **Arne D. Ekstrom**[4], **Nitin Tandon**[1,2,3,*]

[1]Vivian L. Smith Department of Neurosurgery, McGovern Medical School at UT Health Houston, Houston, TX, 77030, United States of America

[2]Texas Institute for Restorative Neurotechnologies, University of Texas Health Science Center at Houston, Houston, TX, 77030, United States of America

[3]Memorial Hermann Hospital, Texas Medical Center, Houston, TX, 77030, United States of America

[4]Department of Psychology, University of Arizona, Tucson, AZ, 85721, United States of America

## Summary

The rapid recognition and memory of faces and scenes implies the engagement of category specific computational hubs in the ventral visual stream with the distributed cortical memory network. To better understand how recognition and identification occur in humans, we performed direct intracranial recordings, in a large cohort of patients (n = 50), from the medial parietal cortex (MPC) and the medial temporal lobe (MTL), structures known to be engaged during face and scene identification. We discovered that the MPC is topologically tuned to face and scene recognition, with clusters in MPC performing scene recognition bilaterally and face recognition in right subparietal sulcus. The MTL displayed a selectivity gradient with anterior, entorhinal cortex showing face selectivity and posterior parahippocampal regions showing scene selectivity. In both MPC and MTL, stimulus specific identifiable exemplars led to greater activity in these cortical patches. These two regions work in concert for recognition of faces and scenes. Feature selectivity and identity sensitive activity in the two regions was coincident and they exhibited theta phase locking during face and scene recognition. These findings together provide clear evidence for a specific role of subregions in the MPC for the recognition of unique entities.

### Keywords

recognition; memory; retrosplenial cortex; posterior cingulate; hippocampus; intracranial recording; gamma; stereoelectroencephalography; subdural grids; prosopagnosia; default network

*Lead contact: nitin.tandon@uth.tmc.edu.

Author Contributions

Conceptualization: OW, NT; Data curation: OW, PSR, KJF, CMK; Software: OW, KJF, CMK; Formal Analysis: OW; Writing – Original Draft: OW; Writing – Review and Editing: OW, NT, ADE; Visualization: OW; Supervision: NT; Project Administration: NT; Funding Acquisition: NT.

Declaration of Interests

The authors declare no competing financial interests

## Introduction

The ability to identify previously encountered people and objects, requires an interplay of activity between sensory and memory regions of the brain. To identify a unique object requires recognizing that it has been encountered before and to be able to retrieve information about it [1-4]. Traditionally, the hippocampus and parahippocampal gyri are implicated as the principal loci subserving these processes [1,5-8]. Distinctive entities such as faces and scenes rely upon specific, category selective constituents of the ventral visual stream and medial temporal lobe (MTL) for recognition.

In recent years it has become clear that the extended memory network underpinning recognition extends beyond the MTL to other regions such as medial parietal cortex (MPC) [9-14]. Prior functional neuro-imaging studies have shown that the MPC is engaged in processing complex scenes [12,15]; path integration [16-18]; spatial memory of landmarks [19,20]; egocentric to allocentric transformation during navigation [21,22] and spatial imagery. It has also been shown to be active in assessments of face familiarity [23-27]. This engagement of MPC in both spatial and facial processing brings up obvious questions regarding its functional organization and its role in recognition. There is some evidence that the MPC engages with known areas of category selectivity within ventral visual pathways [28-33] and the MTL [8,34-37], with known scene and face areas differentially connected to different regions of MPC [27]. Given the role that the MPC is thought to serve as a hub in memory processing, could it also play a role in coordinating category-specific memories alongside the ventral stream?

These questions have been unanswerable till the current time owing to the relative inaccessibility of the medial parietal lobe to time-resolved, electrophysiology (M/EEG), and the infrequency of focal lesions impacting this region [38]. To resolve these questions, we performed intracranial recordings, in a large human cohort, during face and scene identification tasks, using both surface and penetrating electrode arrays. Spatially precise and highly-temporally resolved recordings across a broad region were used to evaluate if MPC is tuned to faces and scenes, and if so, what is its role in recognition and identification relative to the ventral visual stream and the MTL.

## Results

Broadband gamma activity (BGA; 70-150Hz) was recorded using intracranial electrodes in 66 participants (30 male, 18-56 years, 13 left-handed) undergoing intracranial electrode placement for the localization of intractable epilepsy - 18 patients had subdural grid electrodes (SDEs) and 48 had depth recordings using stereotactic EEG electrodes (sEEGs). Participants viewed visual images of famous faces, famous landmarks (scenes) or scrambled images and were asked to name the person or landmark (Figure 1).

### Behavioral Performance

Mean identification accuracy (± SD) was 34 ± 19% for faces and 51 ± 20% for scenes. 16 patients who identified less than 20 face or scene stimuli were excluded from further analysis. Data from the remaining 50 participants, who identified faces and scenes with an

overall accuracy of 39 ± 17% for faces and 56 ± 16% for scenes, were used for further analysis. Articulation latencies for this cohort were; faces 1502 ± 346 ms and scenes 1479 ± 321 ms.

## Category selective regions in MPC: Individual data

Data from two representative patients are shown in Figure 2, each with electrodes in multiple locations within MPC. Each displayed loci with greater activation for one stimulus class over all other categories. TA603 had an SDE grid spanning the extent of the entire right MPC (Figure 2A). Three electrodes, all located over the subparietal sulcus [39], showed prominent BGA increase (>200% above baseline) for faces, with smaller responses (<50%) to other stimulus classes (Figure 2C). Electrode X15, located more posteriorly, responded to both faces and scenes over scrambled stimuli but was not significantly selective to either category. No other electrodes were significantly responsive. A trial-by-trial analysis of activation (Figure 2D) showed a consistent onset time of activation relative to stimulus onset in face selective electrodes that was not strongly coupled to response latency.

TS106 had sEEG electrodes in medial parietal and occipital cortex (Figure 2B). The right subparietal sulcus in this case also showed prominent selectivity for face stimuli. Electrodes located in the parieto-occipital fissure were more active for scene stimuli and, in this case, were scene selective. This separation of preferential activation suggests that MPC processes faces and scenes via spatially distinct neural populations rather than a single, generic cognitive process.

## Face/Scene selectivity in MPC: Population analysis

All 236 electrodes (99 LH, 137 RH), in 39 patients, located within MPC were evaluated for responsivity and selectivity to faces and scenes (Figure 3; Video S1; Video S2; Figure S1), in the 500-1000 ms window. 142 (60%) were responsive, showing significantly greater activation to either faces or scenes than their scrambled versions. Of these, 21 (15%) were face selective, 60 (42%) were scene selective and the remaining 61 (43%) showed no significant differences between these conditions (Figure 3A). There was no significant correlation between the amplitude of face-scene differences and greyscale-color scrambled differences ($r = -0.10$, $p = 0.24$; Figure S2). Face responsive electrodes showed significantly greater activity for whole faces over face parts (Figure S3). In both hemispheres there were a substantial number of electrodes with preferential activation to faces or scenes. Thus, faces and scenes appear to be processed via distinct and only partially overlapping neural substrates in MPC.

To further investigate this spatial separation, we used a mixed-effects multilevel analysis (MEMA) [40]. This method creates an effect size and precision estimate on the cortical surface modelling each electrode's 'recording zone' as an exponentially decaying geodesic radius. A mixed effects analysis of the population is then performed at each node on the cortical surface. This method accounts for sparse sampling, outlier inferences and intra- and inter-subject variability to create a population-level, surface-based representation. This analysis also showed bilateral scene selective cortical clusters superior to the parieto-occipital fissure and in posterior precuneus. In the right hemisphere a well-defined face

selective cluster was seen, anatomically localized to the subparietal sulcus in the right hemisphere, with a small scene selective cluster superior to it (Figure 3C; Video S3).

### Identification sensitivity within category selective regions in MPC

To evaluate the sensitivity of cortical patches in the MPC to the patients' abilities to identity the faces, we compared activation for correctly vs incorrectly answered face naming trials within face selective electrodes and within scene selective electrodes with a significant face response. Of the 21 face selective electrodes, 15 (71%) were face identification sensitive – they showed greater responses for correctly identified faces over incorrectly identified ones (Figure 3D). By contrast, 10 (36%) of the 28 scene selective electrodes with significant face responsiveness showed face identification sensitivity. Of the 60 scene selective electrodes, 22 (37%) were scene identification sensitive (Figure 3F) and only 5 (24%) of the 21 face selective electrodes showed scene identification sensitivity. A multiple linear regression ($r^2 = 0.23$), utilizing all responsive MPC electrodes, revealed that face identity sensitivity was associated with face selectivity ($\beta = 0.94$, $p < 10^{-8}$) and scene identity sensitivity was associated with greater place selectivity ($\beta = -0.28$, $p = 0.046$). This means face and scene selective areas in MPC show preferential activation for known, identifiable exemplars of stimuli they are tuned to. An important question these findings raise is whether this response pattern of selectivity for faces vs. scenes is present in other regions of the cortical memory network. If so, which region shows this phenomenon first?

### Face/Scene selectivity in MTL is similar to MPC

We applied identical analyses to characterize category selectivity and identification sensitivity in the MTL. Of 347 MTL electrodes (192 LH, 155 RH) in 42 patients, 216 (62%) were responsive. Of these, 21 (10%) were face selective, 59 (27%) were scene selective and the remaining 136 (63%) were unselective (Figure 3B). The ratio of face to scene selective electrodes was not significantly different from that in MPC ($\chi^2$ (1, N = 161) = 0.002, p = 0.96). An anterior-posterior separation between face and scene selectivity was noted, with anterior, rhinal areas more likely to show face selectivity and posterior regions showing greater scene selectivity ($r = 0.56$, $p < 10^{-5}$). As in MPC, there was no significant correlation between face-scene and greyscale-color differences ($r = -0.11$, $p = 0.12$; Figure S2) and face responsive electrodes showed significantly greater activity for whole faces over face parts (Figure S3). At the population level, parahippocampal place area was discernable in the right hemisphere (Figure 3C), consistent with previous studies of MTL and ventral visual category selectivity (Figure S4). Of the 21 face selective electrodes, 10 (48%) showed significant face identification sensitivity (Figure 3E). By contrast, 8 (24%) of 34 scene selective, face responsive electrodes were face identification sensitive. As in MPC, a multiple linear regression ($r^2 = 0.14$) revealed that stronger face identity sensitivity was associated with greater face selectivity ($\beta = 0.44$, $p < 10^{-5}$) whereas scene identity sensitivity was associated with greater place selectivity ($\beta = -0.32$, $p < 0.001$).

### MPC and MTL show comparable identification responses to Faces and Scenes

Overall, the statistics for category and identification sensitivity were highly comparable between MTL and MPC. A MEMA contrasting responses during correct and incorrect naming trials for each stimulus type showed sites of identification sensitivity within MPC

and MTL ROIs (Figure 4; Figure S5). We also saw a prominent focus of activation for correct scene and face identity in mid-fusiform cortex, an area we and others have previously shown to be a crucial component of the lexico-semantic retrieval system [41-43]. Activation of the supplementary motor area and anterior cingulate cortex was greater for correct trials, corresponding to speech motor planning and name production.

Of the 142 responsive electrodes in MPC, 53 (37%) showed only face identification sensitivity compared to 45 (32%) with only scene identification sensitivity. 18 (13%) showed significant identification responses to both categories (Figure 5A). Of the 216 responsive electrodes in MTL, 80 (37%) showed face identification sensitivity and 37 (17%) showed scene identification sensitivity. 14 (6%) showed a significant identification response for both categories. The MTL was less engaged in representation of scenes relative to face identification as compared to MPC ($\chi^2$ (1, N = 215) = 4.62, p = 0.032). The right MTL was more specialized for face rather than scene identification than the left MTL (RH 3.64 vs. LH 1.65; $\chi^2$ (1, N = 126) = 3.96, p = 0.046), implying a right MTL lateralization for face recognition. In distinction, MPC showed no lateralization in scene vs. face selectivity (RH 1.56 vs. LH 1.07; $\chi^2$ (1, N = 102) = 0.845, p = 0.36). The time courses of BGA responses of electrodes that were face or scene identification sensitive were remarkably conserved across stimulus categories within each ROI (Figure 5B,C), even though these electrodes were spatially separated. Both regions also showed a beta band (11 – 20 Hz) suppression that reached its trough just after the peak BGA response (Figure 5D).

## Face identification responses in MPC and MTL occur virtually simultaneously

A remaining question is how MPC and MTL interact to enable identification and whether this process occurs earlier in one of the regions. To test this, we evaluated a subset of patients (n = 16) with at least one face identity sensitive electrode in both MPC and MTL. We evaluated two time points within each region; the first time point at which gamma traces were significantly different between faces and scrambled faces and the first point at which they were different for correctly vs incorrectly identified faces. In MPC, median latency for face discrimination was 329 ms (306 - 386 ms, 95% CI) and the latency for identification was 430 ms (403 - 523 ms). In the MTL the latency of face discrimination was 340 ms (311 - 395 ms) and the latency of identification was 425 ms (325 - 488 ms). We generated bootstrapped distributions (Figure 5F) from this analysis to show that peak latencies for each contrast occur near simultaneously in both MPC and MTL. Figure 5G shows the distribution of latency differences in trial-paired MPC and MTL responses. The median difference was −20 ms (−98 – 46 ms) for face determination and 10.5 ms (−80 – 137 ms) for identity. Neither difference was significant (p = 0.77; p = 0.93 respectively). In the subset of patients with at least one scene identify selective electrode in each region (n = 9 patients) the analysis did not show any time points with a significant difference between correct and incorrect trials.

To directly probe the interactions between these regions we measured changes in the phase locking value (PLV) of theta oscillations (3 – 5 Hz) [44-47] between MPC and MTL during these tasks. Of the 1719 within-patient MPC-MTL electrode pairs (n = 33 patients), 108 pairs showed a significant increase in PLV only to faces, 47 pairs only to scenes and 18

pairs significantly increased to both (Figure 6A,B). Face selective pairs showed greater PLV during correct trials than incorrect ($p < 0.001$) or scrambled ($p < 10^{-4}$) trials. Scene selective pairs also showed greater PLV during correct trials than incorrect ($p < 0.01$) or scrambled ($p < 0.001$) trials. Neither face ($p = 0.99$) or scene ($p = 0.77$) selective pairs showed significantly greater PLV for correct over incorrect trials for trials in the category they were non-selective for. Within category selective pairs, the latency for the time points when PLV first became significantly greater for correct vs. incorrect trials was 485 ms for faces (Figure 6C) and 785 ms for scenes (Figure 6D). These findings validate the role of MPC in recognition and imply the existence of category specific functional connectivity between MPC and MTL.

## Discussion

Our work provides clear evidence of a role of MPC in the recognition of unique entities. MPC is topologically tuned to faces and scenes, especially in the right hemisphere, and co-activates and interacts with the MTL. These observations provide evidence that MPC is an important node during recognition – a process it likely helps accomplish via interactions with the hippocampus and MTL. Our thesis is supported by recent imaging studies [48], by lesional analysis of human MPC that result not only in spatial disorientation, but also in concurrent anterograde and retrograde amnesia [11,49-51], and the impact of lesions of the hippocampus resulting in hypoactivity and loss of plasticity of MPC [13,52,53]. The loss of recognition – manifested as the inability to attach name to a face is a common manifestation of normal aging, but is prominently impaired in dementia. The role of the MPC in aging is hinted at by hypometabolism that occurs as a prodrome of Alzheimer's disease [54,55]. Understanding the neurobiology of recognition in the extended cortical memory network is therefore of crucial importance.

The timing of the identification distinction here from neural population recordings (MPC 430 ms; MTL 425 ms) is not dissimilar to the familiarity distinction found from single neuron recordings of human hippocampus (461 ms) [56] suggesting that MPC may play a role in familiarity determination. Our findings are supported by differences seen in activation during fMRI studies of recall of personally familiar over famous people and places [27]. The phase locking between MPC and MTL via theta frequency oscillations [44-47] further provides evidence for the existence of face and scene selective pathways between these regions. That the MPC and MTL are not strongly separable in latency or function is consistent with a strong connectivity between these two regions both anatomically and functionally [57,58], so much so that these regions can be viewed as a distinct, dissociable cortical memory system [12,59], as part of a distributed memory network [60,61].

MPC, particularly retrosplenial cortex [58,62,63], has been most commonly investigated in the context of scene and spatial processing during navigation. However, fMRI studies suggest that it also activates during face presentation [23-26,64]. Our study supports these findings, showing strong responses to faces in MPC. Further, we show regions robustly selective to faces, with a subset of these regions being more engaged during face identification. This selectivity is consistent with previous fMRI studies of category specific recall [27,65], that show an anatomically comparable separation of person and place

information processing. Importantly, by comparing MPC selectivity to MTL we found no difference in the relative ratios of face to scene selective sites – neither of these two regions preferentially represents one stimulus type relative to the other. In both regions we observed a high ratio of scene to face selective electrodes. Given the semi-random sampling within these ROIs this implies that a greater cortical area of both ROIs is dedicated to processing the scene stimuli. This property has previously been observed in fMRI studies of ventral temporal cortex where parahippocampal place area shows larger activation clusters than fusiform face area [66,67].

A well-documented property of the MPC is its involvement in the brain's default network (DN), an interconnected network of brain regions that deactivate during externally directed tasks and activate while constructing internal representations. Recently, the DN has been suggested to be segregable into multiple sub-networks [68-72]. Within MPC there is a repeatable, superior-inferior divide between memberships in these sub-networks that approximately aligns to segregation of our face-scene clusters. The inferior, parieto-occipital fissure scene clusters, can be more broadly considered as part of the network associated with scene processing, navigation and memory-based imagery [68,69,72]. The face cluster, is linked to the network linked to social knowledge, theory of mind and moral decision making [68,71,73].

It could be argued that some of the cortical responses to the faces and scenes stimuli may be confounded by differences in color vs greyscale images. Color is more crucial for scene identity than to face identity [74,75] and was the reason for our choice of these stimuli. However, we find no significant correlation between face-scene and greyscale-color differences in MPC or MTL. Additionally, our results are entirely concordant with previous studies that show regions of MPC selectively activating during text-cued recall of person and place information [27,65]. Also, a number of other episodic memory studies have elicited responses in MPC with text based cues [10,76,77] implying that this is a higher-order region that is mostly invariant to the visual features and perhaps even the modality in which the object is presented.

Given the identification sensitivity seen in this study it appears clear that MPC plays an important role in recognition of faces and scenes, however, it is yet unclear what the unique contributions both MPC and MTL make to these processes. This can be probed using the production of transient lesions using microstimulation, time locked to the activation of each of these regions [78] and may help move us to a true causal understanding of their roles in recognition. Given the timings of activation and the close ties to the activity of the MTL, MPC is most likely involved in some aspect of familiarity. However, an inability to name, as assessed by this task, could be either a lack of familiarity or recollection so this will need further study.

## Conclusions

We have shown, in a large patient cohort, that MPC shows sensitivity to recognition of both faces and scenes in spatially distinct regions that display robust and clear selectivity to either category. We also show, using within-individual comparisons, no distinction in the latency of

these selectivities between MPC and MTL and transient, low frequency interactions between the two regions. Given the lack of strong functional or temporal separability between MPC and MTL, future work should investigate the individual and distinct contributions of each of these nodes of the memory network. Our findings shed new light on the importance of areas outside of those traditionally though to be important to category representation, suggesting the distributed nature of such coding within the human brain.

## STAR Methods

### RESOURCE AVAILABILITY

**Lead Contact—**Further information and requests for resources should be directed to and will be fulfilled by the Lead Contact, Nitin Tandon (nitin.tandon@uth.tmc.edu)

**Materials Availability—**This study did not generate new unique reagents.

**Data and Code Availability—**The datasets generated from this research are not publicly available due to them containing information non-compliant with HIPAA and the human participants the data were collected from have not consented to their public release. However, they are available on request from the corresponding author. The custom code that supports the findings of this study is available from the corresponding author on request.

### EXPERIMENTAL MODEL AND SUBJECT DETAILS

**Participants—**66 patients (30 male, 18-56 years, 13 left-handed) participated in the experiments after giving written informed consent. All participants were semi-chronically implanted with intracranial electrodes for the clinical purposes of seizure localization of pharmaco-resistant epilepsy. Participants with significant additional neurological history (e.g. previous resections, MR imaging abnormalities such as malformations or hypoplasia, or those with prosopagnosia) were excluded. All experimental procedures were reviewed and approved by the Committee for the Protection of Human Subjects (CPHS) of the University of Texas Health Science Center at Houston as Protocol Number: HSC-MS-06-0385.

### METHOD DETAILS

**Electrode Implantation and Data Recording—**Data were acquired from either subdural grid electrodes (SDEs; 18 patients) or stereotactically placed depth electrodes (sEEGs; 48 patients). SDEs were subdural platinum-iridium electrodes embedded in a silicone elastomer sheet (PMT Corporation; top-hat design; 3mm diameter cortical contact), and were surgically implanted via a craniotomy following previously described methods [80-82]. sEEGs were implanted using a Robotic Surgical Assistant (ROSA; Medtech, Montpellier, France) [83]. Each sEEG probe (PMT Corporation, Chanhassen, Minnesota) was 0.8 mm in diameter and had 8-16 electrode contacts. Each contact was a platinum-iridium cylinder, 2.0 mm in length and separated from the adjacent contact by 1.5 - 2.43 mm. Each patient had 12-20 such probes implanted. Following surgical implantation, electrodes were localized by co-registration of pre-operative anatomical 3T MRI and post-operative CT scans in AFNI [84]. Electrode positions were projected onto a cortical

surface model generated in FreeSurfer [85], and displayed on the cortical surface model for visualization [82]. Intracranial data were collected during research experiments starting on the first day after electrode implantation for sEEGs and two days after implantation for SDEs. Data were digitized at 2 kHz using the NeuroPort recording system (Blackrock Microsystems, Salt Lake City, Utah), imported into Matlab, initially referenced to the white matter channel used as a reference for the clinical acquisition system and visually inspected for line noise, artifacts and epileptic activity. Electrodes with excessive line noise or localized to sites of seizure onset were excluded. Each electrode was re-referenced to the common average of the remaining channels. Trials contaminated by inter-ictal epileptic spikes were discarded.

**Stimuli and Experimental Design—**Stimuli were presented using Python v2.7 at a size of 500 x 500 pixels on a 2880 x 1800, 15.4” LCD screen positioned at eye-level, 2-3’ from the patient (~7.5° visual angle). Each stimulus was displayed for 2000 ms with an inter-stimulus interval of 6000 ms. All 66 participants performed famous face and famous landmark (scene) recognition [28]. Participants who correctly identified less than 20 stimuli in either the faces or scenes task were excluded from analysis, 16 participants were excluded this way. 31 patients also performed a face parts classification task, identifying images of eyes, mouths etc. Additional details of each experiment are below:

**Famous Face Recognition:** Participants were presented with greyscale photos of famous faces and asked to verbally name them. Stimuli were presented in one recording session, containing presentation of 90-200 images, consisting of a mix of coherent images and their spatially scrambled versions in a pseudorandom order with no repeats. In trials with scrambled faces the patients were asked to respond with “scrambled”. Data were collected over an eight year period so additional face stimuli were gradually added or replaced throughout the collection period. Stimuli were matched for luminance and contrast using Adobe Photoshop.

**Famous Scene Recognition:** Participants were presented with color photos of famous landmarks (scenes) and asked to verbally recall their location. Stimuli were presented in one recording session, containing presentation of 140-160 images, consisting of a mix of coherent images and their spatially scrambled versions in a pseudorandom order. In trials with scrambled scenes the patients were asked to respond with “scrambled”.

**Face Parts Classification:** Participants were presented with greyscale photos of parts of faces and instructed to verbally name them. Face parts included ears, eyes, mouths and noses. Stimuli were presented in one recording session, containing presentation of 90-100 images, consisting only of coherent images in a pseudorandom order with no repeats.

**Audio Recordings—**Continuous audio recordings were carried out during all experiments with an omnidirectional microphone (30-20,000 Hz response, 73 dB SNR, Audio Technica U841A) placed within 2 feet of the patient, and adjacent to the presentation laptop. These recordings were analyzed offline to manually isolate articulatory onsets and transcribe patient responses. Incorrect responses included either an absence of speech, stating they did not recognize the object or incorrectly identifying the object.

## QUANTIFICATION AND STATISTICAL ANALYSIS

A total of 13,212 electrode contacts were implanted, 4,196 of these were excluded due to proximity to the seizure onset zone, frequent inter-ictal epileptiform spikes or line noise. The remaining 9,016 electrodes were deemed usable. All electrodes within ROIs in MPC and MTL (parahippocampal, perirhinal and entorhinal cortices), based on a brain parcellation derived from the Human Connectome Project [79], were used for further analysis. The MPC ROI comprised of the areas RSC, 7m, POS1, v23ab, d23ab, 31pv and 31pd. The MTL ROI comprised of the areas H, PHA1, PHA2, PHA3, EC, PreS and PeEc. An ROI in ventral occipitotemporal cortex (vOTC) was also used, encompassing all ventral regions not included in the MTL mask (Figure S4).

Raw data recordings from each electrode were bandpass filtered to isolate broadband gamma activity (BGA; 70-150Hz) following removal of line noise (zero-phase 2nd order Butterworth band-stop filters). A frequency domain bandpass Hilbert transform (paired sigmoid flanks with half-width 1.5 Hz) was applied and the analytic amplitude was smoothed (Savitzky - Golay FIR, 3rd order, frame length of 151 ms; Matlab 2017a, Mathworks, Natick, MA). BGA percentage change from baseline, defined as the period 500 to 100ms before visual stimulus presentation in each epoch, was computed.

Electrodes were then evaluated to determine if they were either *Responsive* or *Selective* to the presented stimuli in the 500-1000ms post stimulus onset time window. This window was selected based on the activation latencies of MPC and MTL in previous intracranial studies [44,56]. *Face Responsiveness* (FR) or *Scene Responsiveness* (SR) was determined by computing the z-score of trial-by-trial activity, averaged over the analysis window, for each task against its scrambled control condition. Electrodes with a z-score corresponding to a confidence greater than the Benjamini-Hochberg False Detection Rate (FDR) threshold of $q<0.05$ (calculated across all electrodes) were deemed *stimulus responsive. Selectivity* to Faces/Scenes within these responsive electrodes was determined by testing whether Faces showed a greater response than Scenes. Electrodes with $q<0.05$ and a positive z-score were termed *Face Selective* (FS) and those with a negative z-score were termed *Scene Selective* (SS). *Identification Discrimination* (ID) was determined as electrodes that were more active ($q<0.05$) for correctly identified stimuli against incorrectly identified stimuli. To compute grouped responses across subjects, while minimizing the impact of each individual, within-subject averages of all electrodes within each ROI were calculated and then averaged for the population.

The latency of FR (correct vs. scrambled faces) and Face ID (correct vs. incorrect faces) across ROIs was determined using the latency of the onset of broadband gamma significance that was above threshold for 50 ms. This was computed using a one-tailed Wilcoxon signed rank test applied to within-subject trial averages, tested between 200-700ms post stimulus onset (FDR $q<0.01$ across time points). To validate the separation of these values across regions, a bootstrap analysis with resampling, that used a random selection of 75% of trials from each patient was rerun 1000 times. Trial selection for each repetition was linked in both MPC and MTL to allow a paired analysis of latency differences between regions.

Multiple linear regressions were used to find the association between face and scene identity selectivity and the category selectivity of the electrodes within each ROI. Face vs. scene z-score was modelled as a function of two variables; correct vs. incorrect faces and correct vs. incorrect scenes. Adjusted $r^2$ values are reported.

Phase locking value (PLV) was calculated for patients with electrode coverage in both ROIs (n = 33 patients, 1719 electrode pairs). Phase information was extracted from the down-sampled (200 Hz) and low theta-band filtered signal (3 – 5 Hz; 3rd order, zero-phase Butterworth band-pass filter) [44-46] using a Hilbert transform. PLV was calculated as the circular mean (absolute vector length) of the instantaneous phase difference between each electrode pair at each time point [44] and baselined to the period −500 to −100 ms before stimulus presentation. Statistics were calculated using the mean PLV of correctly answered trials between 500 to 1000 ms after stimulus onset, comparing against a bootstrapped null distribution where MPC and MTL trials were randomly re-paired (2000 iterations). Statistical significance was accepted at an FDR corrected threshold of $q<0.05$. PLV time courses are presented as the between-subject average of all significant electrode pairs within each patient.

To provide statistically robust and topologically precise estimates of BGA, a population-level representation was created using a surface-based mixed-effects multilevel analysis (sb-MEMA) [40,43,81,86,87]. For the MEMAs, results were calculated for the time window 500 to 1000 ms after stimulus onset representing regions with a significant difference between the tested stimuli. A surface-based, geodesic Gaussian smoothing filter (2mm FWHM) was applied. Significance levels were then computed at a corrected alpha of 0.01 using family-wise error rate corrections for multiple comparisons. The minimum criterion for the family-wise error rate was determined by white-noise clustering analysis (Monte Carlo simulations, 1000 iterations) of data with the same dimension and smoothness as that analyzed [40]. Displayed activation clusters were restricted to regions with at least three patients contributing to coverage and BGA difference exceeding 5%. For the MEMA videos, results were calculated for 150 ms windows in 10 ms steps centered from −100 to 1200 ms from stimulus onset. Clusters were restricted to regions with at least three patients contributing to coverage and BGA exceeding 10%.

## Supplementary Material

Refer to Web version on PubMed Central for supplementary material.

## Acknowledgements

We express our gratitude to all the patients who participated in this study; the neurologists at the Texas Comprehensive Epilepsy Program who participated in the care of these patients; and the nurses and technicians in the Epilepsy Monitoring Unit at Memorial Hermann Hospital who helped make this research possible. This work was supported by the National Institute for Deafness and other Communication Disorders DC014589 and National Institute of Neurological Disorders and Stroke NS098981.

## References

1. Yonelinas AP (2002). The nature of recollection and familiarity: A review of 30 years of research. J. Mem. Lang 46, 441–517.

2. Bird CM (2017). The role of the hippocampus in recognition memory. Cortex 93, 155–165. [PubMed: 28654817]
3. Jacoby LL, Toth JP, and Yonelinas AP (1993). Separating Conscious and Unconscious Influences of Memory: Measuring Recollection. J. Exp. Psychol. Gen 122, 139–154.
4. Mandler G (1980). Recognizing: The judgment of previous occurrence. Psychol. Rev
5. Schoemaker D, Mascret C, Collins DL, Yu E, Gauthier S, and Pruessner JC (2017). Recollection and familiarity in aging individuals: Gaining insight into relationships with medial temporal lobe structural integrity. Hippocampus 27, 692–701. [PubMed: 28281326]
6. Schoemaker D, Gauthier S, and Pruessner JC (2014). Recollection and Familiarity in Aging Individuals with Mild Cognitive Impairment and Alzheimer's Disease: A Literature Review. Neuropsychol. Rev 24, 313–331. [PubMed: 25115809]
7. Brambati SM, Benoit S, Monetta L, Belleville S, and Joubert S (2010). The role of the left anterior temporal lobe in the semantic processing of famous faces. Neuroimage 53, 674–681. Available at: 10.1016/j.neuroimage.2010.06.045. [PubMed: 20600979]
8. Martin CB, McLean DA, O'Neil EB, and Kohler S (2013). Distinct Familiarity-Based Response Patterns for Faces and Buildings in Perirhinal and Parahippocampal Cortex. J. Neurosci 33, 10915–10923. Available at: http://www.jneurosci.org/cgi/doi/10.1523/JNEUROSCI.0126-13.2013. [PubMed: 23804111]
9. Cabeza R, and St Jacques P (2007). Functional neuroimaging of autobiographical memory. Trends Cogn. Sci 11, 219–227. [PubMed: 17382578]
10. Gardini S, Cornoldi C, De Beni R, and Venneri A (2006). Left mediotemporal structures mediate the retrieval of episodic autobiographical mental images. Neuroimage 30, 645–655. [PubMed: 16290017]
11. Valenstein E, Bowers D, Verfaellie M, Heilman KM, Day A, and Watson RT (1987). Retrosplenial amnesia. Brain 110, 1631–1646. [PubMed: 3427404]
12. Ranganath C, and Ritchey M (2012). Two cortical systems for memory-guided behaviour. Nat. Rev. Neurosci 13, 713–726. Available at: 10.1038/nrn3338. [PubMed: 22992647]
13. Argyropoulos GP, Loane C, Roca-Fernandez A, Lage-Martinez C, Gurau O, Irani SR, and Butler CR (2019). Network-wide abnormalities explain memory variability in hippocampal amnesia. Elife.
14. Gilmore AW, Nelson SM, and McDermott KB (2015). A parietal memory network revealed by multiple MRI methods. Trends Cogn. Sci 19, 534–543. Available at: 10.1016/j.tics.2015.07.004. [PubMed: 26254740]
15. Silson E, Steel A, and Baker C (2016). Scene selectivity and retinotopy in medial parietal cortex. Front. Hum. Neurosci 10.
16. Knierim JJ (2015). The Hippocampus. Curr. Biol 25, R1116–R1121. [PubMed: 26654366]
17. Chrastil ER, Sherrill KR, Hasselmo ME, and Stern CE (2015). There and Back Again: Hippocampus and Retrosplenial Cortex Track Homing Distance during Human Path Integration. J. Neurosci 35, 15442–15452. Available at: http://www.jneurosci.org/cgi/doi/10.1523/JNEUROSCI.1209-15.2015. [PubMed: 26586830]
18. Hashimoto R, Tanaka Y, and Nakano I (2010). Heading disorientation: A new test and a possible underlying mechanism. Eur. Neurol 63, 87–93. [PubMed: 20090342]
19. Auger SD, Mullally SL, and Maguire EA (2012). Retrosplenial cortex codes for permanent landmarks. PLoS One 7.
20. Epstein RA, Higgins JS, Jablonski K, and Feiler AM (2007). Visual Scene Processing in Familiar and Unfamiliar Environments. J. Neurophysiol 97, 3670–3683. [PubMed: 17376855]
21. Zhang H, Copara M, and Ekstrom AD (2012). Differential Recruitment of Brain Networks following Route and Cartographic Map Learning of Spatial Environments. PLoS One 7.
22. Dhindsa K, Drobinin V, King J, Hall GB, Burgess N, and Becker S (2014). Examining the role of the temporo-parietal network in memory, imagery, and viewpoint transformations. Front. Hum. Neurosci 8.
23. Bernard FA, Bullmore ET, Graham KS, Thompson SA, Hodges JR, and Fletcher PC (2004). The hippocampal region is involved in successful recognition of both remote and recent famous faces. Neuroimage 22, 1704–1714. [PubMed: 15275926]

24. Lee TMC, Leung MK, Lee TMY, Raine A, and Chan CCH (2013). I want to lie about not knowing you, but my precuneus refuses to cooperate. Sci. Rep 3.
25. Gobbini MI, and Haxby JV (2006). Neural response to the visual familiarity of faces. Brain Res. Bull 71, 76–82. [PubMed: 17113931]
26. Visconti Di Oleggio Castello M, Halchenko YO, Guntupalli JS, Gors JD, and Gobbini MI (2017). The neural representation of personally familiar and unfamiliar faces in the distributed system for face perception. Sci. Rep 7. Available at: 10.1038/s41598-017-12559-1.
27. Silson EH, Steel A, Kidder A, Gilmore AW, and Baker CI (2019). Distinct subdivisions of human medial parietal cortex support recollection of people and places. Elife 8.
28. Kadipasaoglu CM, Conner CR, Whaley ML, Baboyan VG, and Tandon N (2016). Category-selectivity in human visual cortex follows cortical topology: A grouped icEEG study. PLoS One 11.
29. Ghuman AS, Brunet NM, Li Y, Konecky RO, Pyles JA, Walls SA, Destefino V, Wang W, and Richardson RM (2014). Dynamic encoding of face information in the human fusiform gyrus. Nat. Commun 5, 5672. [PubMed: 25482825]
30. Tang H, Buia C, Madhavan R, Crone NE, Madsen JR, Anderson WS, and Kreiman G (2014). Spatiotemporal Dynamics Underlying Object Completion in Human Ventral Visual Cortex. Neuron 83, 736–748. [PubMed: 25043420]
31. Gomez J, Barnett M, and Grill-Spector K (2019). Extensive childhood experience with Pokémon suggests eccentricity drives organization of visual cortex. Nat. Hum. Behav 3, 611–624. [PubMed: 31061489]
32. Aguirre GK, Zarahn E, and D'Esposito M (1998). An area within human ventral cortex sensitive to "building" stimuli: Evidence and implications. Neuron 21, 373–383. [PubMed: 9728918]
33. Kanwisher N, Mcdermott J, and Chun MM (1997). The Fusiform Face Area: A Module in Human Extrastriate Cortex Specialized for Face Perception. J. Neurosci 17, 4302–4311. [PubMed: 9151747]
34. Diana RA, Yonelinas AP, and Ranganath C (2008). High-resolution multi-voxel pattern analysis of category selectivity in the medial temporal lobes. Hippocampus 18, 536–541. [PubMed: 18446830]
35. Fairhall SL, Anzellotti S, Ubaldi S, and Caramazza A (2014). Person- and place-selective neural substrates for entity-specific semantic access. Cereb. Cortex 24, 1687–1696. [PubMed: 23425892]
36. O'Craven K, and Kanwisher N (2000). Mental Imagery of Faces and Places Activates Corresponding Stimulus-Specific Brain Regions. J. Cogn. Neurosci 12, 1013–1023. [PubMed: 11177421]
37. Epstein R, and Kanwisher N (1998). A cortical representation of the local visual environment. Nature 392, 598–601. [PubMed: 9560155]
38. Cavanna AE, and Trimble MR (2006). The precuneus: A review of its functional anatomy and behavioural correlates. Brain 129, 564–583. [PubMed: 16399806]
39. Ono M, Kubik S, and Abernathey C (1990). Atlas of the Cerebral Sulci (New York: Thieme Medical Publishers Inc.).
40. Kadipasaoglu CM, Baboyan VG, Conner CR, Chen G, Saad ZS, and Tandon N (2014). Surface-based mixed effects multilevel analysis of grouped human electrocorticography. Neuroimage 101, 215–224. [PubMed: 25019677]
41. Binder JR, Desai RH, Graves WW, and Conant LL (2009). Where is the semantic system? A critical review and meta-analysis of 120 functional neuroimaging studies. Cereb. Cortex 19, 2767–2796. [PubMed: 19329570]
42. Conner CR, Chen G, Pieters TA, and Tandon N (2014). Category specific spatial dissociations of parallel processes underlying visual naming. Cereb. Cortex 24, 2741–2750. [PubMed: 23696279]
43. Forseth KJ, Kadipasaoglu CM, Conner CR, Hickok G, Knight RT, and Tandon N (2018). A lexical semantic hub for heteromodal naming in middle fusiform gyrus. Brain 141, 2112–2126. [PubMed: 29860298]
44. Foster BL, Kaveh A, Dastjerdi M, Miller KJ, and Parvizi J (2013). Human Retrosplenial Cortex Displays Transient Theta Phase Locking with Medial Temporal Cortex Prior to Activation during Autobiographical Memory Retrieval. J. Neurosci 33, 10439–10446. [PubMed: 23785155]

45. Fuentemilla L, Barnes GR, Düzel E, and Levine B (2014). Theta oscillations orchestrate medial temporal lobe and neocortex in remembering autobiographical memories. Neuroimage 85, 730–737. Available at: 10.1016/j.neuroimage.2013.08.029. [PubMed: 23978597]
46. Solomon EA, Kragel JE, Sperling MR, Sharan A, Worrell G, Kucewicz M, Inman CS, Lega B, Davis KA, Stein JM, et al. (2017). Widespread theta synchrony and high-frequency desynchronization underlies enhanced cognition. Nat. Commun 8. Available at: 10.1038/s41467-017-01763-2.
47. Watrous AJ, Tandon N, Conner CR, Pieters T, and Ekstrom AD (2013). Frequency-specific network connectivity increases underlie accurate spatiotemporal memory retrieval. Nat. Neurosci 16, 349–356. Available at: 10.1038/nn.3315. [PubMed: 23354333]
48. Schedlbauer AM, Copara MS, Watrous AJ, and Ekstrom AD (2014). Multiple interacting brain areas underlie successful spatiotemporal memory retrieval in humans. Sci. Rep 4, 6431. [PubMed: 25234342]
49. Maeshima S, Osawa A, Yamane F, Yoshihara T, Kanazawa R, and Ishihara S (2014). Retrosplenial amnesia without topographic disorientation caused by a lesion in the nondominant hemisphere. J. Stroke Cerebrovasc. Dis 23, 441–445. Available at: 10.1016/j.jstrokecerebrovasdis.2013.03.026. [PubMed: 23608367]
50. Maeshima S, Ozaki F, Masuo O, Yamaga H, Okita R, and Moriwaki H (2001). Memory impairment and spatial disorientation following a left retrosplenial lesion. J. Clin. Neurosci 8, 450–451. [PubMed: 11535016]
51. McDonald CR, Crosson B, Valenstein E, and Bowers D (2003). Verbal Encoding Deficits in a Patient with a Left Retrosplenial Lesion. Neurocase 7, 407–417.
52. Garden DLF, Massey PV, Caruana DA, Johnson B, Warburton EC, Aggleton JP, and Bashir ZI (2009). Anterior thalamic lesions stop synaptic plasticity in retrosplenial cortex slices: expanding the pathology of diencephalic amnesia. Brain 132, 1847–1857. [PubMed: 19403787]
53. Albasser MM, Poirier GL, Warburton EC, and Aggleton JP (2007). Hippocampal lesions halve immediate-early gene protein counts in retrosplenial cortex: Distal dysfunctions in a spatial memory system. Eur. J. Neurosci 26, 1254–1266. [PubMed: 17767503]
54. Nestor PJ, Fryer TD, Ikeda M, and Hodges JR (2003). Retrosplenial cortex (BA 29/30) hypometabolism in mild cognitive impairment (prodromal Alzheimer's disease). Eur. J. Neurosci 18, 2663–2667. [PubMed: 14622168]
55. Minoshima S, Giordani B, Berent S, Frey KA, Foster NL, and Kuhl DE (1997). Metabolic reduction in the posterior cingulate cortex in very early Alzheimer's disease. Ann. Neurol 42, 85–94. [PubMed: 9225689]
56. Rutishauser U, Ye S, Koroma M, Tudusciuc O, Ross IB, Chung JM, and Mamelak AN (2015). Representation of retrieval confidence by single neurons in the human medial temporal lobe. Nat. Neurosci 18, 1041–1050. Available at: 10.1038/nn.4041. [PubMed: 26053402]
57. Kahn I, Andrews-Hanna JR, Vincent JL, Snyder AZ, and Buckner RL (2008). Distinct Cortical Anatomy Linked to Subregions of the Medial Temporal Lobe Revealed by Intrinsic Functional Connectivity. J. Neurophysiol 100, 129–139. Available at: http://jn.physiology.org/cgi/doi/10.1152/jn.00077.2008. [PubMed: 18385483]
58. Chrastil ERR, Tobyne SMM, Nauer RKK, Chang AEE, and Stern CEE (2018). Converging meta-analytic and connectomic evidence for functional subregions within the human retrosplenial region. Behav. Neurosci 132, 339–355. [PubMed: 30321025]
59. Baldassano C, Esteva A, Fei-Fei L, and Beck DM (2016). Two distinct Scene-Processing networks connecting vision and memory. eNeuro 3.
60. Schedlbauer A, and Ekstrom A (2017). Memory and Networks: Network-Based Approaches to Understanding the Neural Basis of Human Episodic Memory. In Learning and Memory: A Comprehensive Reference (Elsevier), pp. 99–111. Available at: 10.1016/B978-0-12-805159-7.03005-9.
61. Kim K, Ekstrom AD, and Tandon N (2016). A network approach for modulating memory processes via direct and indirect brain stimulation: Toward a causal approach for the neural basis of memory. Neurobiol. Learn. Mem 134, 162–177. Available at: 10.1016/j.nlm.2016.04.001. [PubMed: 27066987]

62. Nasr S, Liu N, Devaney KJ, Yue X, Rajimehr R, Ungerleider LG, and Tootell RBH (2011). Scene-selective cortical regions in human and nonhuman primates. J. Neurosci 31, 13771–13785. [PubMed: 21957240]
63. Vann SD, Aggleton JP, and Maguire EA (2009). What does the retrosplenial cortex do? Nat. Rev. Neurosci 10, 792–802. [PubMed: 19812579]
64. Wang Y, Metoki A, Smith DV, Medaglia JD, Zang Y, Benear S, Popal H, Lin Y, and Olson IR (2020). Multimodal mapping of the face connectome. Nat. Hum. Behav Available at: 10.1038/s41562-019-0811-3.
65. Peer M, Salomon R, Goldberg I, Blanke O, and Arzy S (2015). Brain system for mental orientation in space, time, and person. Proc. Natl. Acad. Sci. U. S. A 112, 11072–11077. [PubMed: 26283353]
66. Golarai G, Ghahremani DG, Whitfield-Gabrieli S, Reiss A, Eberhardt JL, Gabrieli JDE, and Grill-Spector K (2007). Differential development of high-level visual cortex correlates with category-specific recognition memory. Nat. Neurosci 10, 512–522. [PubMed: 17351637]
67. Golarai G, Liberman A, Yoon JMD, and Grill-Spector K (2010). Differential development of the ventral visual cortex extends through adolescence. Front. Hum. Neurosci 3, 1–19.
68. Braga RM, and Buckner RL (2017). Parallel Interdigitated Distributed Networks within the Individual Estimated by Intrinsic Functional Connectivity. Neuron 95, 457–471.e5. Available at: 10.1016/j.neuron.2017.06.038. [PubMed: 28728026]
69. Andrews-Hanna JR (2012). The brain's default network and its adaptive role in internal mentation. Neuroscientist 18, 251–270. [PubMed: 21677128]
70. Buckner RL, and DiNicola LM (2019). The brain's default network: updated anatomy, physiology and evolving insights. Nat. Rev. Neurosci 20, 593–608. Available at: http://www.ncbi.nlm.nih.gov/pubmed/31492945. [PubMed: 31492945]
71. DiNicola LM, Braga RM, and Buckner RL (2020). Parallel distributed networks dissociate episodic and social functions within the individual. J. Neurophysiol 123, 1144–1179. [PubMed: 32049593]
72. Andrews-Hanna JR, Reidler JS, Sepulcre J, Poulin R, and Buckner RL (2010). Functional-Anatomic Fractionation of the Brain's Default Network. Neuron 65, 550–562. Available at: 10.1016/j.neuron.2010.02.005. [PubMed: 20188659]
73. Mars RB, Neubert FX, Noonan MAP, Sallet J, Toni I, and Rushworth MFS (2012). On the relationship between the "default mode network" and the "social brain." Front. Hum. Neurosci 6, 1–9. [PubMed: 22279433]
74. Gegenfurtner KR, and Rieger J (2000). Sensory and cognitive contributions of color to the recognition of natural scenes. Curr. Biol 10, 805–808. [PubMed: 10898985]
75. Liu CH, and Chaudhuri A (1997). Face recognition with multi-tone and two-tone photographic negatives. Perception 26, 1289–1296. [PubMed: 9604064]
76. Foster BL, Dastjerdi M, and Parvizi J (2012). Neural populations in human posteromedial cortex display opposing responses during memory and numerical processing. Proc. Natl. Acad. Sci 109, 15514–15519. Available at: http://www.pnas.org/cgi/doi/10.1073/pnas.1206580109. [PubMed: 22949666]
77. Natu VS, Lin JJ, Burks A, Arora A, Rugg MD, and Lega B (2019). Stimulation of the Posterior Cingulate Cortex Impairs Episodic Memory Encoding. J. Neurosci 39, 7173–7182. [PubMed: 31358651]
78. Moore BD, Aron AR, and Tandon N (2018). Closed-loop intracranial stimulation alters movement timing in humans. Brain Stimul. 11, 886–895. Available at: 10.1016/j.brs.2018.03.003. [PubMed: 29598890]
79. Glasser MF, Coalson TS, Robinson EC, Hacker CD, Harwell J, Yacoub E, Ugurbil K, Andersson J, Beckmann CF, Jenkinson M, et al. (2016). A multi-modal parcellation of human cerebral cortex. Nature 536, 171–178. [PubMed: 27437579]
80. Tandon N (2012). Mapping of human language. In Clinical Brain Mapping, Yoshor D and Mizrahi E, eds. (McGraw Hill Education), pp. 203–218.
81. Conner CR, Ellmore TM, Pieters TA, Disano MA, and Tandon N (2011). Variability of the Relationship between Electrophysiology and BOLD-fMRI across Cortical Regions in Humans. J. Neurosci 31, 12855–12865. [PubMed: 21900564]

82. Pieters TA, Conner CR, and Tandon N (2013). Recursive grid partitioning on a cortical surface model: an optimized technique for the localization of implanted subdural electrodes. J. Neurosurg 118, 1086–1097. [PubMed: 23495883]

83. Tandon N, Tong BA, Friedman ER, Johnson JA, Von Allmen G, Thomas MS, Hope OA, Kalamangalam GP, Slater JD, and Thompson SA (2019). Analysis of Morbidity and Outcomes Associated With Use of Subdural Grids vs Stereoelectroencephalography in Patients With Intractable Epilepsy. JAMA Neurol. 76, 672–681. [PubMed: 30830149]

84. Cox RW (1996). AFNI: Software for Analysis and Visualization of Functional Magnetic Resonance Neuroimages. Comput. Biomed. Res 29, 162–173. [PubMed: 8812068]

85. Dale AM, Fischl B, and Sereno MI (1999). Cortical Surface-Based Analysis: I. Segmentation and Surface Reconstruction. Neuroimage 9, 179–194. [PubMed: 9931268]

86. Fischl B, Sereno MI, and Dale AM (1999). Cortical Surface-Based Analysis: II: Inflation, Flattening, and a Surface-Based Coordinate System. Neuroimage 9, 195–207. [PubMed: 9931269]

87. Kadipasaoglu CM, Forseth K, Whaley M, Conner CR, Rollo MJ, Baboyan VG, and Tandon N (2015). Development of grouped icEEG for the study of cognitive processing. Front. Psychol 6.

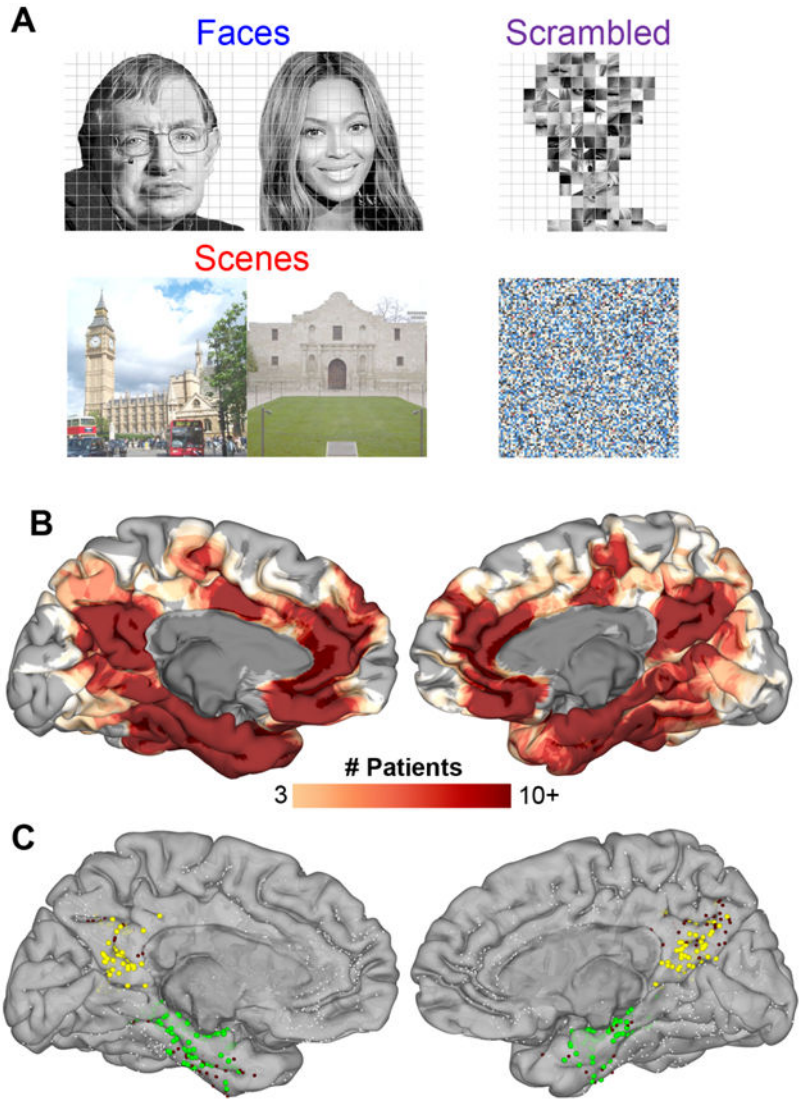


**Figure 1. Task and Patients.**

(A) Representative stimuli for each stimulus category. (B) Spatial coverage represented as a heat map on a standardized N27 brain surface showing extensive and consistent coverage of the medial parietal cortex and medial temporal lobe (n = 50 patients that performed both face and scene identification correctly). (C) Individual electrode locations (9,016 total electrodes) highlighting electrodes in the two ROIs defined using a parcellation derived from the Human Connectome Project [79]. Responsive electrodes are shown in MPC (yellow, n = 142) and MTL (green, n = 216). Electrodes within these ROIs not responsive to either faces or scenes are in maroon and electrodes outside these two ROIs are in white

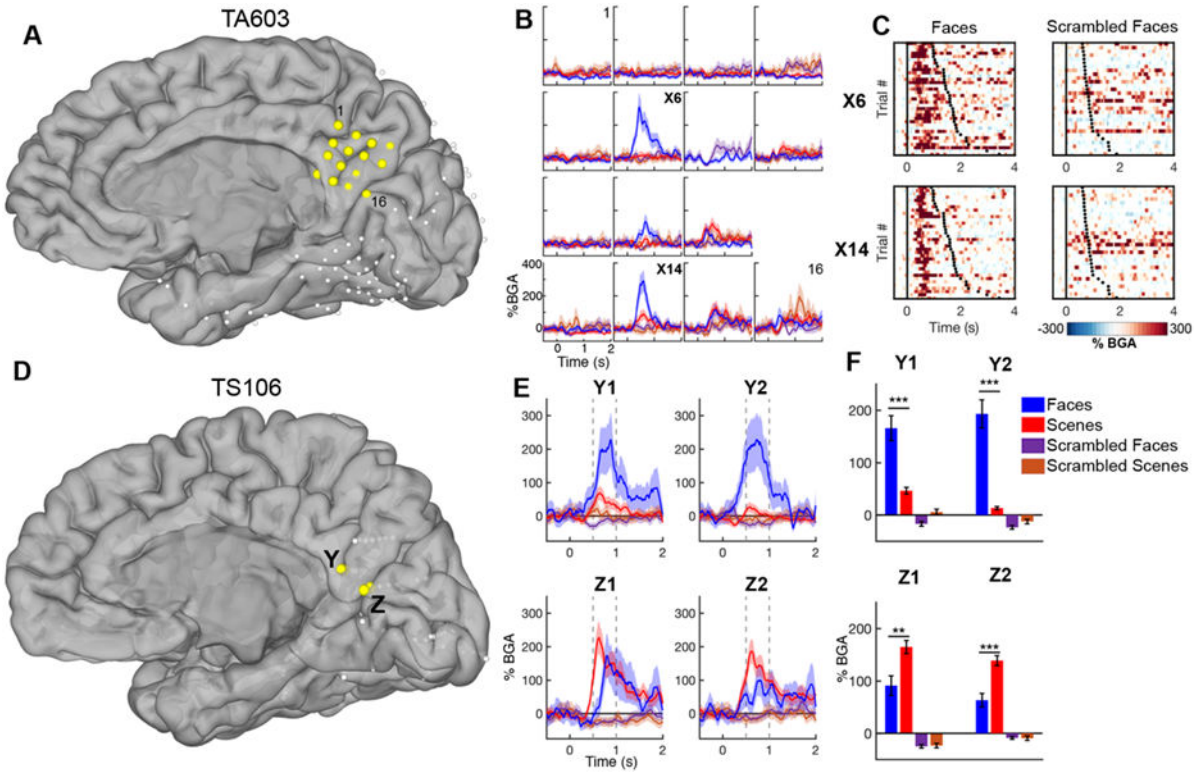


**Figure 2. MPC category selectivity – individual analysis.**

(A,D) Electrode locations in two representative patients - plotted electrodes are in yellow. (B) Time course (mean ± SEM) of BGA at each electrode in the MPC SDE grid in response to each stimulus category. (C) Raster plots of single trial BGA in response to faces (left) and scrambled faces (right) for two electrodes. Trials are organized by response latency with black dots representing time of articulation onset. (E) Time course of BGA at four sEEG electrodes. Vertical dashed lines indicate time windows used for selectivity analyses. (F) Selective responses for faces and scenes, 500-1000 ms post stimulus onset, at the same four electrodes. ** $p<0.01$, *** $p<0.001$.

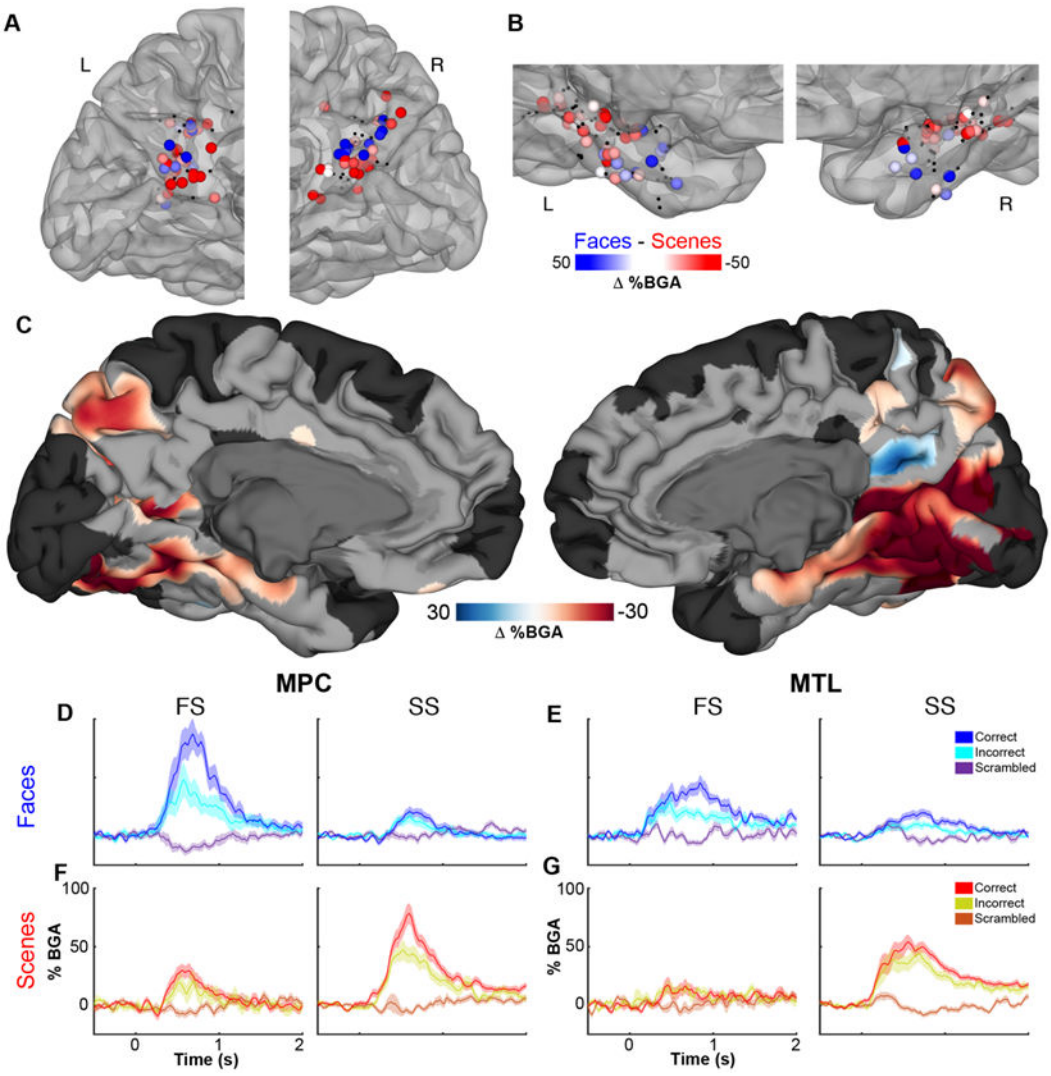


**Figure 3. Category selectivity in MPC and MTL – population analysis.**

Selectivity of responses in (A) MPC and (B) MTL for faces (blue) and scenes (red) in the time window of 500-1000 ms after stimulus onset (See also Figures S1 - S3). Non-selective electrodes ($q>0.05$) are black. (C) A population-level, surface-based MEMA contrasting (faces vs. scrambled faces) – (scenes vs. scrambled scenes) revealing regions of significant stimulus selectivity ($p<0.01$ corrected) in the ventral visual stream (See also Figure S4) and medial parietal cortex (See also Videos S1 - S3). Regions in black did not have consistent coverage for reliable MEMA results. Between-patient averaged BGA (mean ± SEM) in MPC (D,F) and MTL (E,G) at face selective (FS) or scene selective (SS) electrodes. Face (D,E) and scene (F,G) identification sensitivity in FS electrodes and SS electrodes.

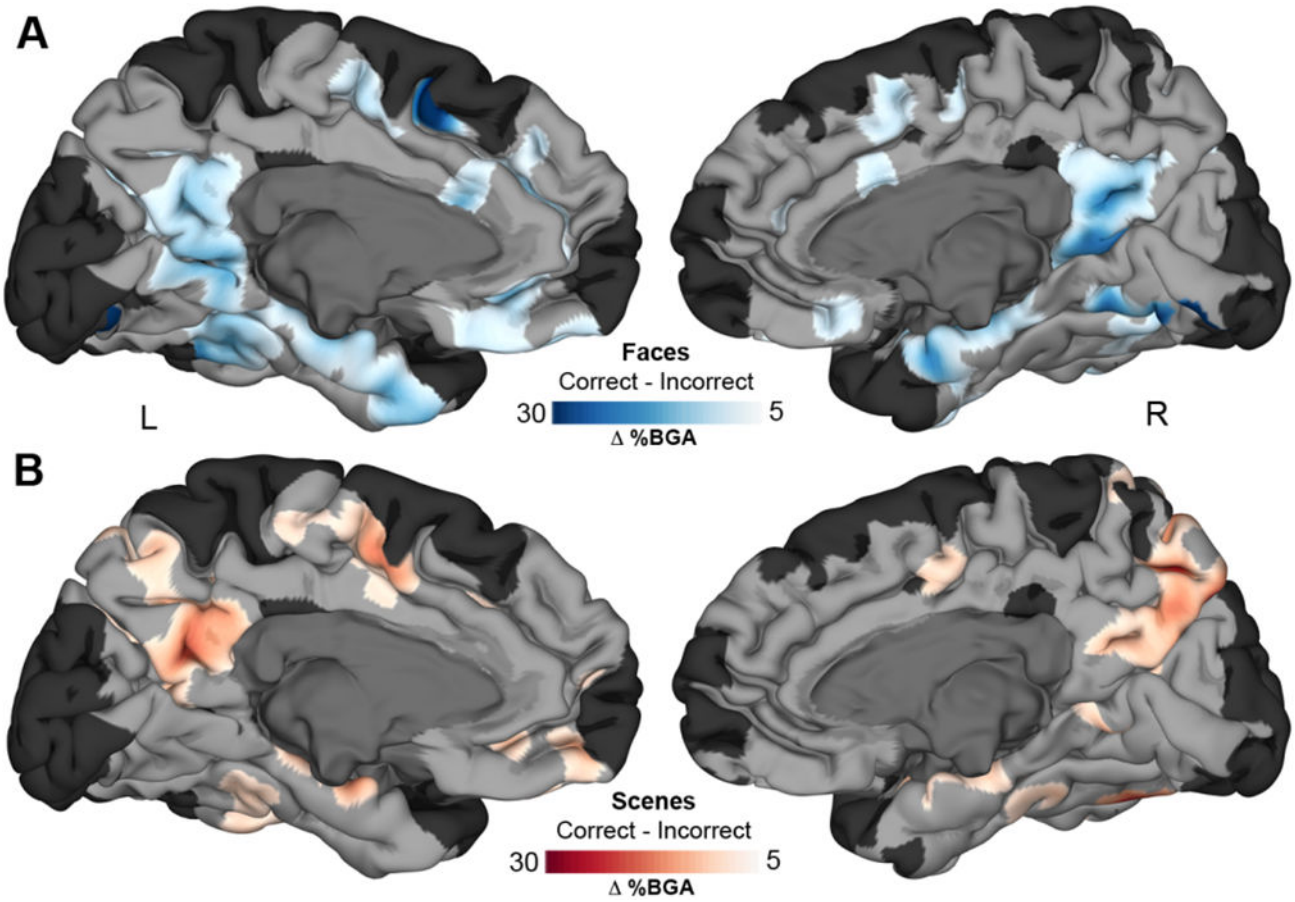


**Figure 4. All-patient maps of identification sensitivity.**

MEMA representation of selectivity to correct over incorrect naming trials of faces (A) and scenes (B). Regions in MPC and MTL show significant identification sensitivity ($p<0.01$ corrected) for each stimulus category (See also Figure S5). Regions in black did not have consistent coverage for reliable MEMA results.

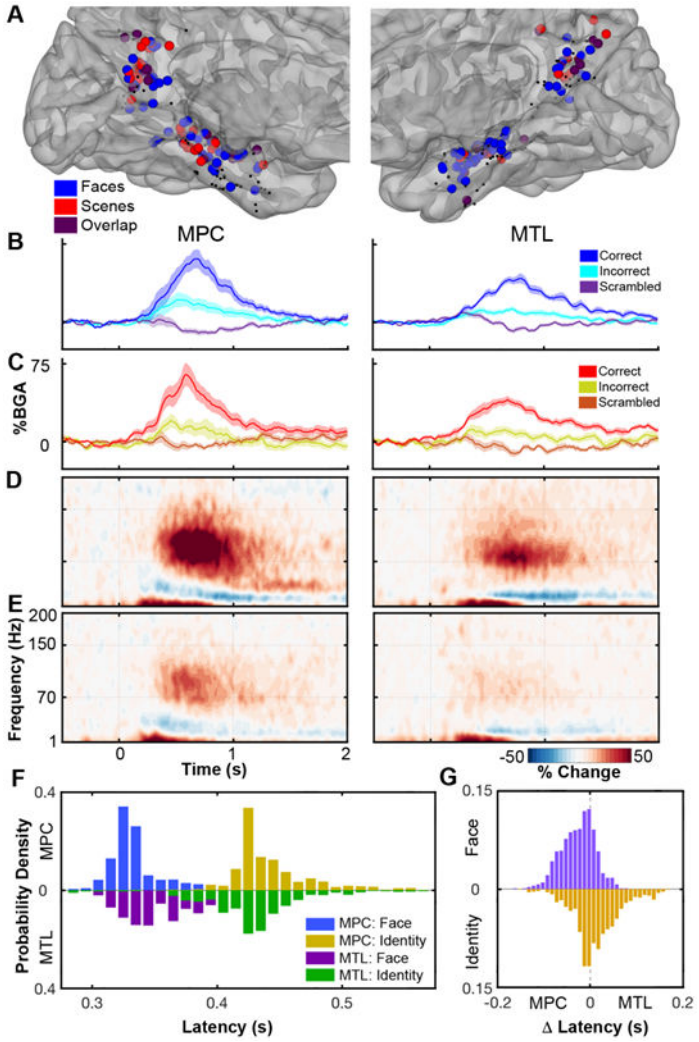


**Figure 5. Identity sensitivity in MPC and MTL.**

(A) Co-localization of identity selective electrodes ($q<0.05$) for face (blue) and scene (red) stimuli, and their overlap (purple), in MPC and MTL. Non-selective electrodes are black. Averaged BGA time courses (mean ± SEM) for face (B) and scene (C) identity sites. Grouped spectrograms showing broadband changes in face identity electrodes for correctly (D) and incorrectly (E) identified faces. (F) Bootstrap distribution determining the initial latency when it is possible to distinguish a face from a scrambled face or a known face from an unfamiliar one based on the BGA in both MPC and MTL. (G) Distribution of paired latency difference between regions.

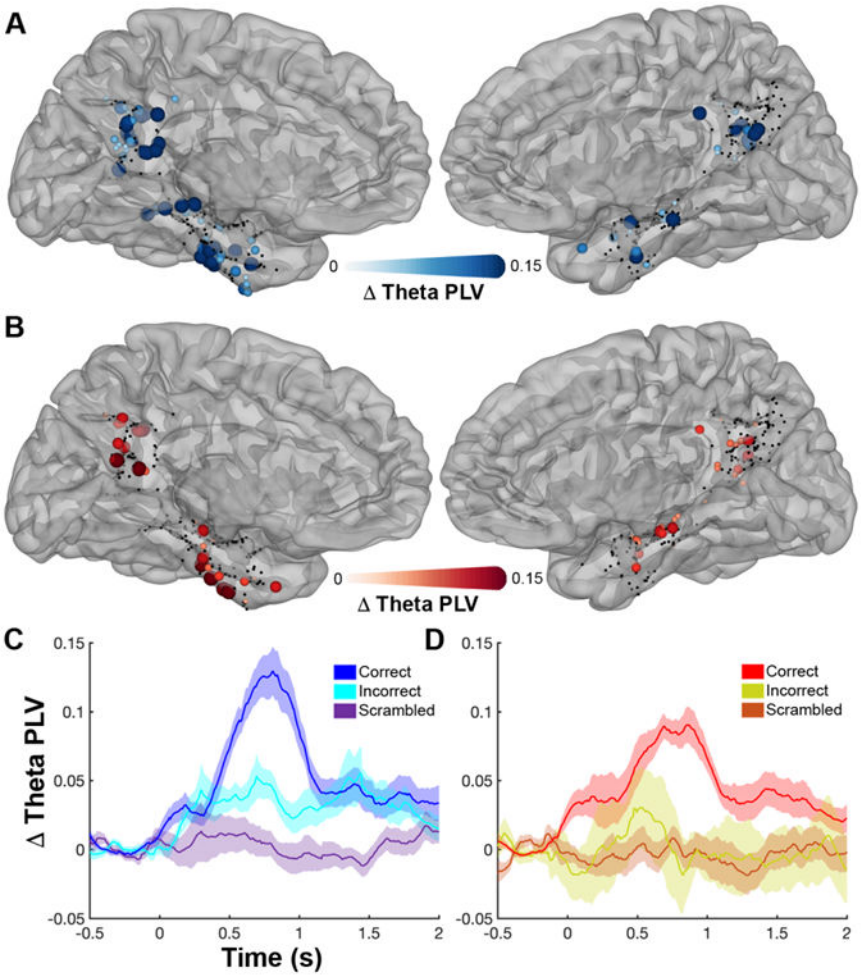


**Figure 6. Theta Phase Locking between MPC and MTL.**

Localization of electrodes significantly involved (q<0.05) in inter-regional theta phase coupling in the faces (A) and scenes (B) tasks. Non-significant electrodes are black. Average time courses (mean ± SEM) of PLV changes from baseline between the significant face (C; 14 patients) and scene (D; 11 patients) pairs.